Investigating the Influence of Dynamic Jet Shapes on the Jet Electrochemical Machining Process

Matthias Hackert*,[1], Gunnar Meichsner[2], Stephan F. Jahn [1], Andreas Schubert[1,2]
[1]Chemnitz University of Technology, Chair Micromanufacturing Technology
[2]Fraunhofer Institute for Machine Tools and Forming Technology, Chemnitz
*09107 Chemnitz, Germany, matthias.hackert@mb.tu-chemnitz.de

Abstract: Electrochemical Machining is a potential procedure for micro manufacturing technology. Especially the absence of machining forces makes it advantageous for processing metals with high hardness and for the generation of complicated geometries. Applying a closed electrolytic free jet (Jet Electrochemical Machining - Jet-ECM) the electric current is restricted to a limited area. That allows working gaps of about 100 µm and makes Jet-ECM suitable for manufacturing feature sizes in sub micrometer scale [1, 2]. Using transient COMSOL Multiphysics models the Jet-ECM spot machining process can be simulated [3]. By comparing the results of simulation and experiment, a good coincidence especially for small aspect ratios have been found out. At higher aspect ratios the coincidence diminishes. One possible reason is the assumption of a static shape of the jet while processing in the FEM model. To increase the quality of the simulation in this study the up to now neglected interaction of the free jet with the erosion shape was implemented in the model.

Keywords: Jet Electrochemical Machining, localized anodic dissolution, closed electrolytic free jet

1 Introduction

Jet Electrochemical Machining (Jet-ECM) is a technology to generate complex microstructures by help of anodic dissolution. Defined volumes of material can be removed from metallic workpieces by applying an electric direct current at an electrolyte jet, ejected from a small nozzle. The removal depends on the effective current density which amounts up to 1000 A/cm^2. This high current density is locally restricted by the shape of the jet and working gaps down to 100 µm between workpiece and nozzle can be used.

Jet-ECM is a fast technology for creating complex 3D micro geometries into metallic parts without any thermal or mechanical impact and independent from the material's hardness. The processed surface is very smooth and no tool wear occurs.

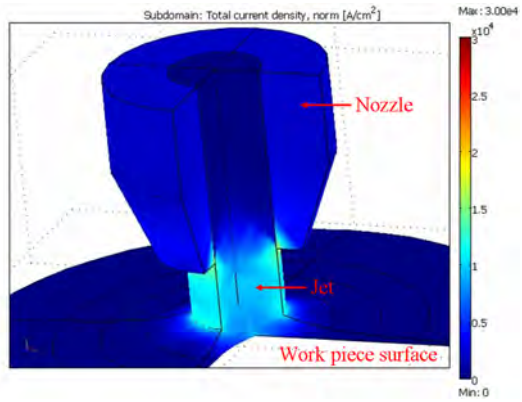

Figure 1: Jet-ECM model in 3D.

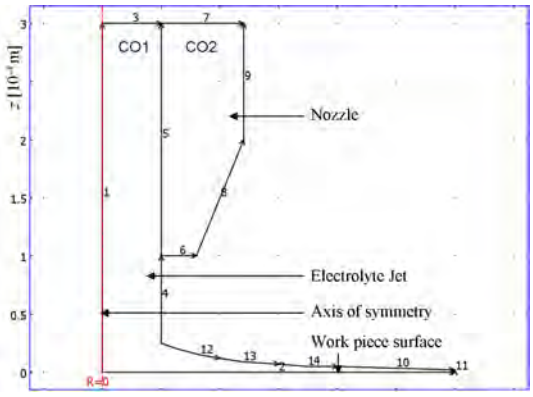

Figure 2: Jet-ECM model 2D axial-symmetric.

One major parameter for the process simulation which influences the results strongly is the jet shape. However, it is hardly to predict or control. Yoneda and Kunieda showed a rotational symmetric stationary model of Jet-ECM for a smooth surface at time zero

[4]. From this work the geometries of nozzle, jet, and workpiece surface shown in Figures 1 and 2 were derived, implemented into COMSOL Multiphysics, and simulations for process times up to 2 s were conducted [3]. But compared to experimental work the results differ with increasing process time. Reason for this is probably the static jet shape applied in the model. For an improved prediction of resulting geometries the up to now neglected interaction of the electrolyte surface with the machined geometrie need to be simulated as well. The simulation of the Jet-ECM process with such a dynamic jet shape is presented in the following.

2 Geometry, Mesh, and Physics

The Jet-ECM process was implemented as transient axial-symmetric 2D model into the COMSOL application modes "Moving Mesh" and "Conductive Media DC". A nozzle with a diameter of 100 µm ejects a jet onto a substrate placed in a distance of 100 µm. The workpiece' surface at time zero is the abscissa. The jet diameter d_{jet} is equal with the nozzle diameter and the electrolyte film on the surface at $t = 0$ decreases degressively starting from $0.25\, d_{jet}$, following the Jet-ECM model of Yoneda and Kunieda [4] (Figure 2). The mesh was generated using the automatic mesh creator with the option "Extra fine" and consists of 2,537 elements.

Boundary	Definition
1	Axial symmetry
2	$\varphi = 56$ V
3	$\varphi = 0$ V
4	$\vec{n}_A \cdot \vec{J} = 0$
5	Continuity
6	$\vec{n}_A \cdot \vec{J} = 0$
7	$\varphi = 0$ V
8–14	$\vec{n}_A \cdot \vec{J} = 0$

Table 1: Boundary conditions for the boundaries numbered in Figure 2.

In subdomain CO1 (cf. Figure 2), which represents the electrolyte, an isotropic electric conductivity was defined with the experimental value of 16 S/m. CO2 was chosen out of the COMSOL's material library as steel AISI 4340 with a conductivity of $4.032 \cdot 10^6$ S/m. All electric boundary conditions are shown in Table 1, where φ is the electric potential, $\vec{n}_A$ is the normal vector, and $\vec{J}$ is the current density. The total voltage of 56 V over the working gap conforms the used power of the applied current supply, which has a sufficient maximum output of 1 A.

The anodic dissolution which takes place on boundary 2 is defined as mesh displacement corresponding to Faraday's law with a velocity in normal direction $\vec{v}_n$ depending to the normal current density $\vec{J}_n$ as shown in equation 1. The parameters are shown in Table 2.

$$\vec{v}_n = \eta \cdot \frac{M}{z_A \cdot \rho \cdot F} \cdot \vec{J}_n \qquad (1)$$

	Name	Value
η	Current efficiency	100 %
M	Molar mass	55.06 g/mol
z_A	Valency	3.436
ρ	Mass density	7.76 g/cm^3
F	Faraday constant	$9.65 \cdot 10^4$ C/mol

Table 2: Variables in equation 1 and used values for the simulated and machined stainless steel 1.4541.

The current efficiency η for Jet-ECM spot processing of stainless steel 1.4541 was found out experimentally and amounts 100 % [3].

By starting the solver the resulting geometry is represented by a calotte-shaped deformation of boundary 2.

The shape of the electrolyte surface for $t > 0$ depends on the resulting substrate geometry. A static electrolyte boundary leads to an unrealistic increase of the electrolyte volume over the formed pit and therefore to a wider pit [3]. The real movement of the electrolyte surface depends on fluidic conditions interacting with the created pit geometry. To evaluate the real fluidic conditions of the process the jet needs to be considered as flowing media which makes the model too complex. The first simple but effective approach, that could be applied into the model, was to allow the electrolyte boundaries 10, 12, 13, 14 a free movement i. e. to preset no mesh displacement or mesh velocity. Boundary 4 was set to zero jet displacement in radial direction and no restrictions in axial direction.

3 Results and Discussion

The simulations were made up to 0.7 s processing time with a step size of 0.1 s. Figure 3 and 4 show the difference in pit and jet shaping for the model with static (Figure 3) and dynamic (4) electrolyte boundary at $t = 0.4\,s$.

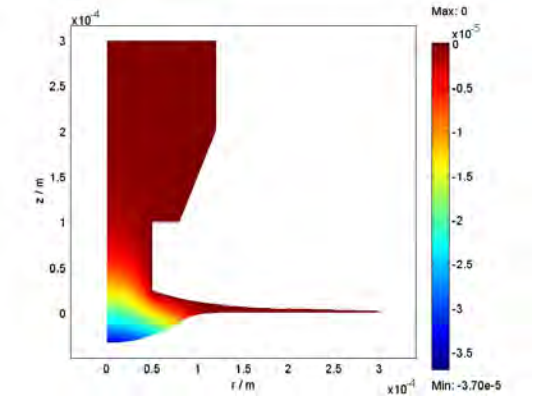

Figure 3: Surface plot of z-displacement at $t = 0.4\,s$ for a static electrolyte boundary.

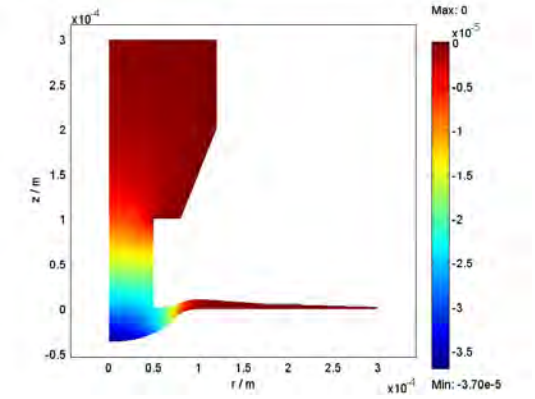

Figure 4: Surface plot of z-displacement at $t = 0.4\,s$ for a dynamic electrolyte boundary.

In the model with a free electrolyte boundary a movement of the electrolyte edge towards the substrate is visible. This characteristic can be observed as well in experiments. In Figures 5 and 6 the normal current densities at the substrate's boundary are depicted which are proportional to the displacement of boundary (equ. 1). Thus, one can predict that the pit forming will differ for the moving electrolyte boundary compared to the static electrolyte shape.

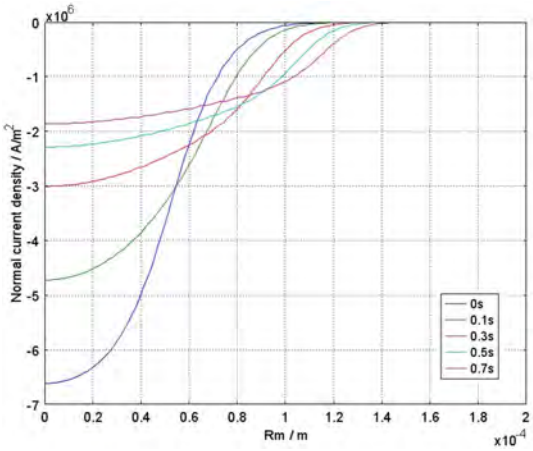

Figure 5: Current densities at the substrate boundary for the static electrolyte boundary.

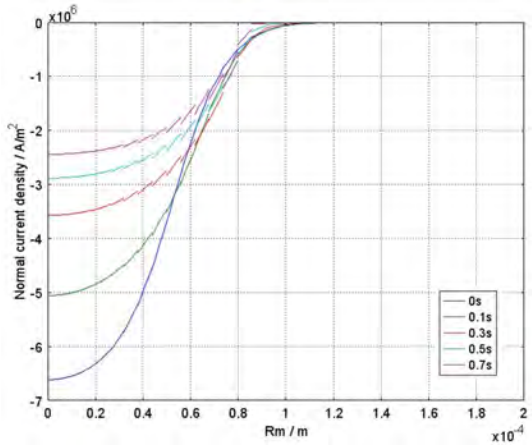

Figure 6: Current densities at the substrate boundary for the dynamic electrolyte boundary.

The shapes of machined calottes were measured with tactile profiling. The simulated geometries for both models are compared to experimental results in Figure 7. Like expected from the current density plot, the geometry deviations between the dynamic electrolyte boundary simulations to the experimentally generated pits are smaller than to the static boundary simulations. Indeed, the simulations with the static electrolyte boundary are closer to reality concerning the pit depth (Figure 8). But regarding the pit diameter (Figure 8), the dynamic electrolyte boundary leads to a better coincidence with the experiments.

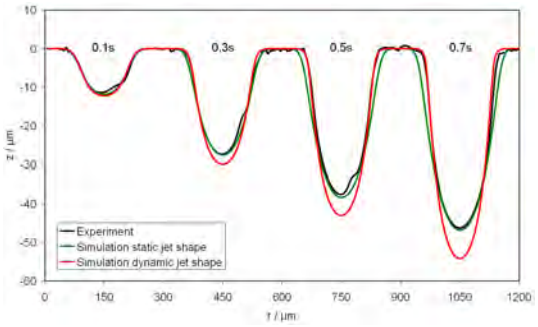

Figure 7: Comparison of simulated and experimentally generated Jet-ECM pit geoemtries.

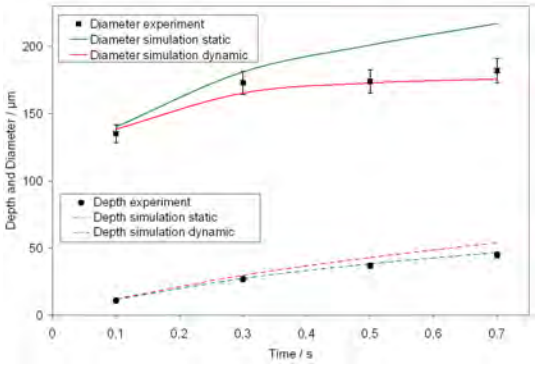

Figure 8: Comparison of pit depth and diameter of simulated and experimentally generated Jet-ECM point erosions.

The model with the dynamic electrolyte boundary comes closer to reality than the static boundary. However, the model is only valid for short time scales. Applying longer process times the simulation leads to undercut geometries due to strong thinning of the electrolyte film at the pit perimeter.

The definition of an electrolyte geometry depending on the in-situ-generated substrate geometry would enable the definition of a more realistic model without a remarkable increase of calculation effort. A simple approach to get closer to reality would be to set a constant distance in z direction between the electrolyte boundary and the substrate. But this option is not available in the used application modes.

4 Conclusion

In this study the influence of a dynamic jet shape on the Jet-ECM process was simulated. The simulation results were compared with results of modelling with a static jet shape and with experimental results.

The results of the dynamic jet shape model are an improvement to the static jet shape in comparison the practical experiments at pit geometries. For time scales up to 0.7 s the coincidence to reality is much better than for the static electrolyte boundary. It could be verified that the simulation with dynamic jet shape shows the same localization of the dissolution process like the experimental results. The increased difference in the pit depth may be caused by transition resistances or other effects which will be topic of further investigations.

References

[1] M. Hackert, G. Meichsner, and A. Schubert. Generating micro geometries with air assisted jet electrochemical machining. *Proceedings of the euspen 10th Anniversary International Conference*, 2:420–424, 2008.

[2] W. Natsu, T. Ikeda, and M. Kunieda. Generating complicated surface with electrolyte jet machining. *Precision Engineering*, 31:33–39, 2007.

[3] M. Hackert, G. Meichsner, and A. Schubert. Simulation of the shape of micro geometries generated with jet electrochemical machining. *Proceedings of the European COMSOL Conference 2008*.

[4] K. Yoneda and M. Kunieda. A numerical analysis of cross sectional shape of microindents formed by the electrochemical jet machining. *J JSEME*, 29.

Acknowledgements

The authors thanks the German Research Foundation for the financial support.